High-Pressure Study of Two Polymorphs of 2,4,6-Trinitrotoluene Using Neutron Powder Diffraction and Density Functional Theory Methods

A High-Pressure Study of Two Polymorphs of TNT Using Neutron Powder Diffraction and DFT Methods

Sumit Konar,*† Adam A. L. Michalchuk,† Nilgun Sen,† Craig L. Bull,‡ Carole A. Morrison,† and Colin R. Pulham†

†EaStCHEM School of Chemistry and Centre for Science at Extreme Conditions, The University of Edinburgh, King's Buildings, David Brewster Road, Edinburgh EH9 3FJ, U.K.

‡ISIS Neutron and Muon Facility, STFC Rutherford Appleton Laboratory, Harwell, Oxford, Didcot, Oxfordshire OX11 0QX, U.K.

KEYWORDS. Neutron diffraction, Rietveld refinement, Equation of state, High pressure, Energetic materials, Trinitrotoluene, Hydrostatic

ABSTRACT: A high-pressure neutron diffraction study was conducted on polycrystalline samples of the two known polymorphs of 2,4,6-trinitrotoluene [monoclinic (m-) and orthorhombic (o-) TNT] under hydrostatic conditions. Isothermal equations of state were obtained for both polymorphic forms. Neither polymorph was observed to undergo a phase transition in the pressure region 0–5 GPa, with both polymorphs displaying smooth compression behavior across the pressure range. This differs somewhat from previous XRD and Raman spectroscopy investigations in which discontinuities were observed in the *P-V* curves and spectral changes were reported at ~2 GPa. The high-pressure response of these materials is supported by dispersion-corrected DFT calculations which, while overestimating the experimental bulk moduli, give excellent agreement with the observed smooth compression response of both phases.

INTRODUCTION

Energetic materials (EMs), exemplified by propellants, explosives and pyrotechnics, release large amounts of energy when initiated by mechanical, electrostatic, or thermal stimuli.[1] The mechanism by which this energy is released involves a complex interplay of chemical and physical phenomena. Hence, understanding and predicting the response of an EM to a mechanical perturbation is non-trivial.[2] A complete model for the reaction of an EM requires consideration of the initial energy generation, its localization[3–6] and influence on chemical reaction mechanisms,[7,8] molecular decomposition kinetics,[9] and a thorough understanding of how the reaction front propagates through the solid material. Many of these phenomena are closely related to the mechanical response of the material. Furthermore, relatively low pressures are known to induce structural changes (polymorphism) in molecular materials.[10,11] These transformations can have considerable effects on the reactivity (e.g. sensitivity) of an EM,[12] and may influence the propagation of a shock front. Understanding the initiation and reaction propagation in EMs therefore requires a detailed understanding of the pressure response of the material. Molecular EMs, including FOX-7[10], HMX[13,14], RDX[15–17], and TATB[18] have all been investigated under high-pressure conditions; many of them undergo pressure-induced phase transitions .

2,4,6-trinitrotoluene (TNT) is one of the most widely used secondary explosives, and was the main explosive used throughout the First World War. It is known to exist in two polymorphic forms under ambient conditions:[19] (1) the thermodynamically stable monoclinic form, m-TNT (space group = $P2_1/a$, Z =8), and (2) the metastable orthorhombic form, o-TNT (space group = $Pca2_1$, Z=8) as shown in Figure 1. TNT does not contain hydrogen bond donor or acceptor sites, and the crystal structures are thus dominated by weak van der Waals interactions. It follows that changes in molecular packing have minimal enthalpic consequence and mixtures of the two polymorphic forms occur readily.[19]

Despite the discovery of the two polymorphs in the 1950s, the structural relationship between them has remained poorly understood for decades. In 1994

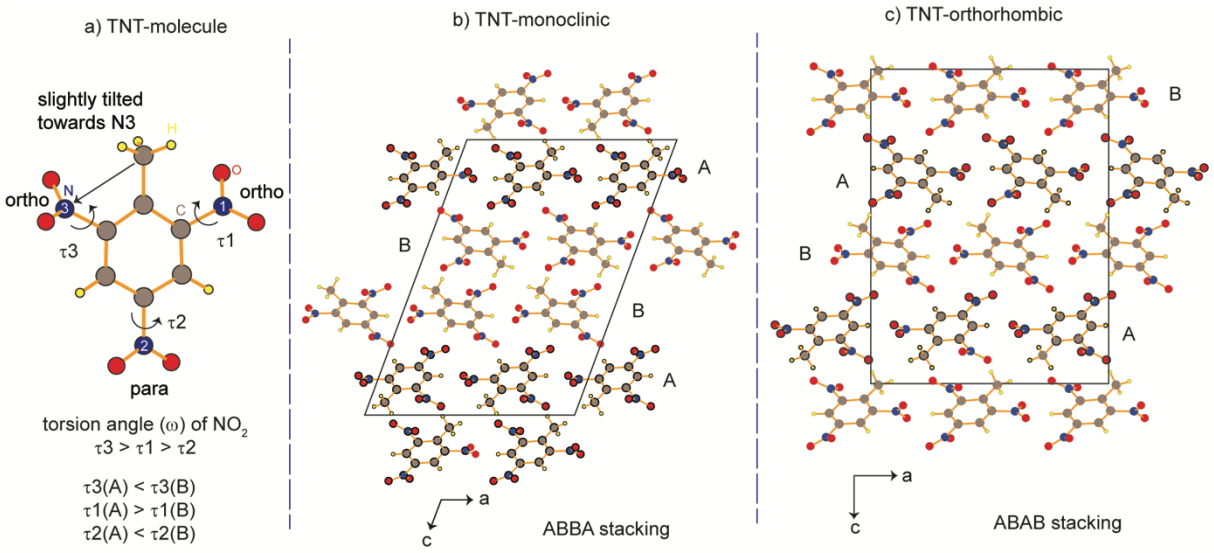

Figure 1 a) Labelling of two structurally distinct molecules (A and B) of TNT identified in the crystal structures; unit cells of b) the monoclinic and c) orthorhombic forms of TNT.

Golovina et al. reported the first clear description for the packing of the two structures.[20] The full structural characterisation was only reported in 2003 by Vrcelj et al who used single crystal X-ray diffraction (SXRD).[19] Figure 1 shows the molecular arrangements in the two polymorphs of TNT in which there are two geometrically distinct molecular conformations (labelled A and B), which differ primarily in the torsion angles of their -NO_2 groups with respect to the planar aromatic ring. In both A and B, steric factors require that the torsion angles of the two ortho-NO_2 groups (τ1 and τ3) in Figure 1 are larger than that of the para-NO_2 group (τ2 in Figure 1). The methyl group tilts slightly (ca 2°) towards one of the ortho -NO_2 groups (labelled 3 in Figure 1), with the torsion angle of the three -NO_2 groups following the order τ3> τ1> τ2. The structures of m- and o-TNT differ primarily in the stacking of molecules with A and B geometries, as shown in Figure 1.

The stability of TNT over a wide temperature range makes it suitable for use as a melt-cast explosive.[21] Upon casting, however, the metastable o-TNT modification is often produced alongside m-TNT. The subsequent o-TNT → m-TNT phase transition, which occurs upon storage, leads to formation of macroscopic defects (cracks, voids, etc.). This in turn causes mechanical instabilities, permitting the formation of potential hot spots within the bulk, and hence a mechanism for sensitization of the material. Pressure-induced transformations may also be important in bulk compositions, where local stresses at fracture tips or during compaction can be high. Thus, in addition to offering insight into the initiation and detonation properties of EMs, understanding the polymorphic phase diagram of TNT is crucial for controlling the macroscopic integrity of its compositions.

The equation of state (EoS) of m-TNT has previously been determined under non-hydrostatic conditions using angle dispersive X-ray diffraction (XRD) at room temperature.[22] This study suggested that a phase transition from m-TNT → o-TNT occurs at ~20 GPa, preceded by a "subtle cusp" in the P-V/V_0 curve near 4 GPa. However, due to the limited number of data points at p > 20 GPa, no EoS was determined for o-TNT. Recently, Bowden et al. performed in situ synchrotron XRD and vibrational spectroscopic measurements at room temperature to investigate the phase stability of m-TNT up to 18 GPa.[23] Up to 2 GPa the predominantly lattice-based modes (i.e. ν < 250 cm^{-1}) showed large mode Grüneisen parameters, with multiple modes found to split with increasing pressure. This large pressure dependence has been suggested to account for considerable adiabatic heating upon mechanical impact, and thus large excitation of the crystal lattice.[24] The large variation in ν was assigned to the significant unit-cell volume collapse (~ 13%) between 0 and 2 GPa, associated with compression primarily along the crystallographic c-axis. However, due to the non-hydrostatic conditions of the experiment, the data quality was insufficient for full structural refinement and gave large uncertainties in the determined crystal lattice parameters.

X-ray crystallographic studies of powdered organic materials are often hindered by the low atomic number of their constituent atoms (C, H, N, O) and the low symmetries of their crystallographic structures. As a result, X-ray scattering experiments generally result in very many low-intensity Bragg reflections. This provides a significant obstacle to obtaining reliable structural parameters for the pressure evolution of the crystal. While these problems can be largely mitigated by use of synchrotron radiation sources, it has been shown that high energy sources can lead to photo-

induced molecular decomposition in some materials. This is exemplified by CL-20, which was severely damaged by synchrotron X-rays which rendered unit cell determination impossible.[25] This can be circumvented through the use of neutron diffraction techniques which have become important tools for the study of these reactive materials.[25]

Due to the important connection between an energetic material's structural behavior upon compression and its properties upon initiation, considerable effort has also been devoted to the development of theoretical frameworks for their prediction.[26,27] First principles simulation (Density Functional Theory, DFT) has demonstrated a remarkable ability to predict the mechanical properties of EMs, particularly when weak dispersion forces are accounted for.[27] The continued validation of increasingly sophisticated dispersion models is therefore an important step towards the ab initio prediction of EM properties.

The objectives of the present work presented are:(i) to undertake a hydrostatic compression study using neutron powder diffraction (NPD) to obtain accurate pressure-volume equations of state for the two known polymorphs of TNT; (ii) to explore the capacity of modern DFT models to predict the hydrostatic compression behavior of two polymorphs of TNT, and in turn be used as a tool to guide experimental endeavors; (iii) to explore detailed structural changes suspected to occur near 2 GPa in the monoclinic form, and (iv) explore for the first time the effect of pressure on the metastable orthorhombic phase of TNT.

EXPERIMENTAL AND COMPUTATIONAL METHODS

2.1. Preparation of TNT-d_5

CAUTION! TNT is a powerful secondary explosive material that should only be prepared and handled by trained personnel using the appropriate safety precautions.

A nitrating mixture of fuming nitric acid (Sigma-Aldrich, 6 mL 99.5%) and sulfuric acid (Fischer Scientific, 17.5 mL ≥ 95%) was prepared and cooled to -5 °C using a POLAR BEAR PLUS CRYSTAL (Cambridge Reactor Design). Toluene-d_8 (4.5 mL; D 99.5%) was added drop wise over a period of 1 h, ensuring that temperatures remained < 0 ºC. The solution was stirred for a further 30 min at -5 °C. The reaction mixture was slowly raised to 70 °C (with a heating rate 1 °C/min) and held at this temperature for 1 h. The sample was heated further to 90 °C for 45 min and then to 100 °C for 45 min. The mixture was subsequently cooled to ambient temperature and held in an ice bath (-10 °C) for 15 min. The product was extracted [20 mL chloroform-d1 (99.8 atom % D)] and neutralised with 5% $NaHCO_3$ in D_2O. Upon drying, TNT-d_5 was obtained. The extent of deuteration and nitration was verified by ^1H NMR. The resulting TNT powder was found to crystallize as the metastable orthorhombic form after rapid evaporation. A pure sample of the thermodynamically stable monoclinic form was obtained by slurrying a mixture of the orthorhombic and monoclinic forms overnight in perdeuterated ethanol. The phase purity of both forms was confirmed by laboratory X-ray powder diffraction (XRPD) using Cu K_α radiation, and by Raman spectroscopy using a Jobin-Yvon LabRam 300 spectrometer equipped with a 50 mW He-Ne laser of wavelength 632.8 nm. Both the XRPD and Raman spectroscopy measurements were performed by enclosing the powder in 0.5 mm diameter borosilicate glass capillaries.

2.2. Neutron Powder Diffraction (NPD).

High-pressure time-of-flight neutron-diffraction measurements were performed on the PEARL instrument[28] at the ISIS Neutron and Muon Source, UK. Pressure was generated by means of a V3 variant Paris-Edinburgh (P-E) press[29] with single-toroidal zirconia-toughened alumina (ZTA) anvils, up to a maximum pressure of ~5 GPa. A null-scattering TiZr gasket was used[30] and hydrostatic pressure conditions were maintained by the inclusion of a mixture of perdeuterated pentane/iso-pentane as the pressure-transmitting media (PTM).[31] This was chosen in preference to perdeuterated ethanol/methanol on account of the appreciable solubility of TNT in ethanol/methanol. A small piece of lead foil was included in the sample volume to act as a pressure calibrant.[32] Neutron-diffraction data were collected in approximately 2.5-tonne steps up to a maximum applied load of 57.5 tonnes. A beamline-developed correction for the wavelength and scattering-angle dependence of the neutron attenuation by the anvil (ZTA) and gasket materials was applied to the measured pattern. The data were normalised using MANTID[33] and Rietveld refinement of the data was performed using the GSAS package.[34] Rietveld refinement was carried out at each pressure point, refining the scale, lattice parameters and peak profiles against the experimental powder diffraction pattern. Constraints were imposed such that thermal vibration parameters are refined collectively for each atom type. The data were of sufficient quality to permit refinement of the atomic co-ordinates of the TNT molecules in both forms, provided the molecules were treated as rigid bodies. Principal axes (a unique set of orthogonal axes) upon compression were obtained using the program PASCAL .[35]

2.3 Computational Details:

Plane-wave Density Functional Theory (PW-DFT) calculations were performed using CASTEP[36] v17.21, with input structures taken from the previously reported ambient pressures structures for each phase.[19] The structures were initially optimized without the application of an external applied stress; high-pressure structures were generated by subsequent optimization under an applied stress, incrementally increased by 0.5 GPa. All calculations were performed using the DFT

functional of Perdew-Burke-Ernzerhof (PBE),[37] with either Grimme's D2[38] or Tkatchenko-Scheffler (TS) dispersion correction[39], PBE-D2 and PBE-TS, respectively. The PBE-D2 approach has been previously shown to perform well for similar nitro-based EMs under hydrostatic compression.[10] CASTEP 'on-the-fly' pseudopotentials were used throughout, and the wave function was expanded in plane waves to a kinetic energy cut-off of 1000 eV. The electronic structure was sampled in reciprocal space using a Monkhorst-Pack (MP) grid,[40] with spacing 0.035 $Å^{-1}$. Optimisation was stopped when a total energy convergence < 10^{-8} eV, atomic displacement < 10^{-3} Å, forces < 10^{-2} eV/Å and stress < 10^{-2} GPa were achieved. While the DFT-D2 dispersion scheme was selected here on account of its prevalence in previous EM literature, we do note that newer developments have been made, namely as DFT-D3 and DFT-D4.[41,42]

3. RESULTS AND DISCUSSION

3.1 Overview of two polymorphs at ambient pressure:

TNT has been recrystallized from a wide range of organic solvents, and the role of solvent in the production of both polymorphs has been studied extensively.[43] In this work, metastable o-TNT was readily obtained by rapid evaporation from chloroform. Obtaining a pure sample of m-TNT proved challenging, as slow evaporation (over a couple of days) consistently produced a mixture of the two crystal forms from a range of organic solvents (Figure 2a). A phase-pure sample of m-TNT was only obtained when a mixture of the two forms was slurried overnight in ethanol. This confirms the thermodynamic stability of m-TNT under ambient conditions. The extent of deuteration and nitration was verified by ^{1}H NMR (Figure S1, ESI). Raman spectra (measured between 100 – 2000 cm^{-1}) of perdeuterated samples of both m-TNT and o-TNT were found to be indistinguishable and are consistent with the previous Raman study on solid m-TNT sample (which were based on hydrogenated materials).[44] . Figure 2b shows the Raman spectra of two samples and a selection of Raman band assignments: i. C-CD_3 stretching (1194 cm^{-1}), ii. nitro symmetric stretching (1351-1373 cm^{-1}); iii. nitro asymmetric stretching (1530-1545 cm^{-1}), and iv. C–C aromatic stretching (1603 cm^{-1}); the respective assignments for hydrogenated m-TNT sample are 1208, 1356, 1543, 1618 cm^{-1}, respectively.[44]

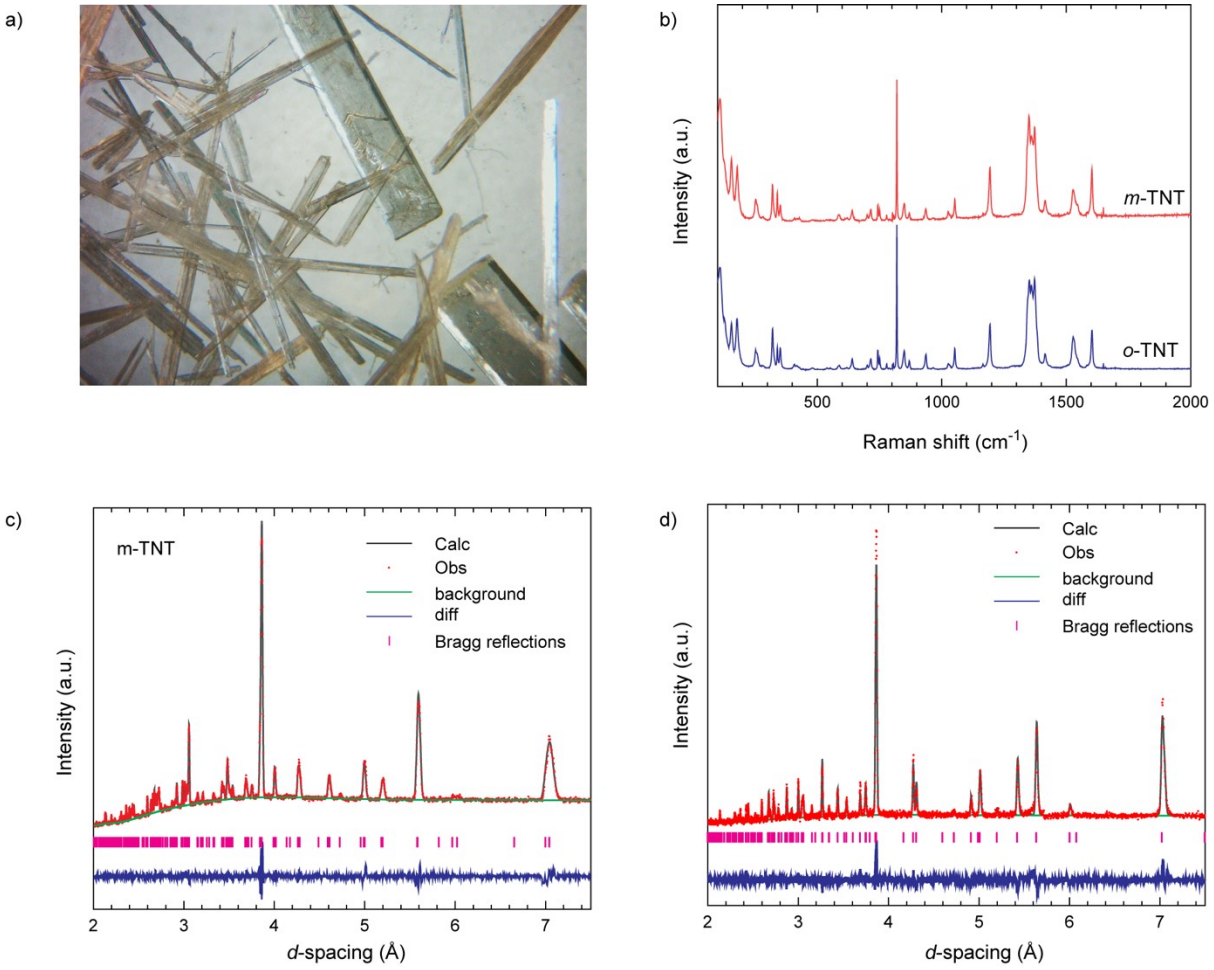

Figure 2 a) Photograph of mixture of the mixed crystal phases of TNT (perdeuterated), b) Raman spectra of both forms m-TNT and o-TNT (perdeuterated); c)-d) Rietveld refinements of the powder X-ray patterns (obtained using laboratory diffractometer using Cu Kα radiation) for both m-TNT and o-TNT samples (perdeuterated) at ambient pressure.

Table 1. Crystallographic data for both *m*- and *o*-TNT, along with data from two literature SXRD studies for comparison. Data obtained from DFT geometry optimization with the D2 and TS dispersion schemes are also shown as PBE-D2 and PBE-TS, respectively.

Polymorph	Lattice parameter	This work			Vrcelj et al [19]	Golovina et al.[20]
		XRPD[a] (298 K)	PBE-D2 (0 K)	PBE-TS (0 K)	SXRD m-TNT [100 K] o-TNT [123 K]	SXRD [295 K]
m-TNT ($P2_1/a$)	a (Å)	14.9978(5)	15.065	15.120	14.9113(1)	15.019(8)
	b (Å)	6.0831(1)	6.057	6.070	6.0340(1)	6.0932(5)
	c (Å)	21.2522(4)	20.848	21.270	20.8815(3)	21.41(2)
	β (°)	110.133(2)	111.218	111.429	110.365(1)	111.00(2)
	V ($Å^3$)	1820.42(6)	1773.310	1817.137	1761.37(4)	1829(2)
	Z	8	8	8	8	8
o-TNT ($Pca2_1$)	a (Å)	14.9921(9)	15.026	15.0784	14.910(2)	15.013(8)
	b (Å)	6.0763(4)	5.998	6.0430	6.0341(18)	6.0836(5)
	c (Å)	20.0320(7)	19.632	19.9604	19.680(4)	20.04(2)
	V ($Å^3$)	1824.8(2)	1769.180	1818.77	1770.58(70)	1830(2)
	Z	8	8	8	8	8

[a] Obtained from Rietveld refinement of laboratory PXRD of deuterated TNT ($C_7D_5N_3O_6$) at ambient temperature

.

A recent computational study[45] has calculated the terahertz vibrational spectrum for the two forms. This suggested that the two polymorphs do exhibit differences at low energies, below the limit of our Raman spectra.

Rietveld refinements were performed using the XRPD data-sets for both m-TNT and o-TNT samples (perdeuterated) at ambient pressure, Figures 2(c)-(d). The crystallographic parameters of both polymorphs as obtained under ambient conditions from laboratory XRPD measurements are given in Table 1 and are in good agreement with literature reports.[20] The values obtained from PBE-D2 and PBE-TS optimization of the unit cells are also tabulated for comparison. In all cases, the DFT geometry optimization simulations inherently neglect thermal contributions and hence correspond to 0 K structures. Methods are available which account for thermal expansion (*via* molecular dynamics or the quasi-harmonic approximation), and in some cases may play a decisive role in determining mechanical properties.[46] However, these methods remain highly computationally demanding and are outside the scope of the present work. Neglecting thermal expansion is often not problematic for materials that exhibit minimal thermal expansion, literature reports suggest TNT expands considerably with temperature.[19] For example, m-TNT has a unit-cell volume of 1761.37(4) $Å^3$ at 100 K, increasing by ca. 3% to 1820.42(6)$Å^3$ at 298 K. It is therefore not surprising to find that the PBE-D2 calculations also underestimate the ambient temperature unit cell volume by ca 3%. It is worth noting that this underestimation is predominantly the result of underestimating the crystallographic c-axis length. This axis is in the direction of the largest

Table 2. Torsion angles of the three -NO_2 groups (τ1, τ2 and τ3 in deg) in molecules A & B, according to literature SXRD studies and DFT calculations (this study) at 0 and 5 GPa, with varying dispersion correction scheme

			Golovina et al [0 GPa][20]	Vrcelj et al [0 GPa][19]	PBE-D2 (0 GPa)	PBE-TS (0 GPa)	PBE-D2 (5 GPa)	PBE-TS (5 GPa)
m-TNT	A	τ1	46	44	43	44	42	43
		τ2	22	23	24	23	24	22
		τ3	50	52	49	49	55	52
	B	τ1	41	38	38	38	37	36
		τ2	32	35	34	35	37	38
		τ3	60	59	57	60	60	59
o-TNT	A	τ1	47	49	43	44	41	41
		τ2	22	28	25	23	23	22
		τ3	54	58	52	52	56	55
	B	τ1	41	39	38	38	37	36
		τ2	33	33	34	35	37	38
		τ3	56	59	58	60	59	59

proportion of void space and is therefore most responsive to temperature effects (See Table 1). The TS dispersion correction yields an improved reproduction of the room temperature structural parameters, which suggests that the TS correction scheme is overestimating the effects of dispersion for this crystal structure. The same is observed for o-TNT (Table 1). Our PBE-TS calculated lattice constants are in excellent agreement with a previous study.[45]

The torsion angles for the -NO_2 groups of the A and B molecules in both polymorphic forms (as obtained from the PBE-D2 and PBE-TS) are tabulated in Table 2 and compared with previous studies. The -NO_2rotational barriers for an isolated molecule of TNT have been previously reported.[44] In the lowest energy gas phase structure, the ortho-NO_2 groups adopt values of $\tau = 35^o$, with the rotational barrier to $\tau = 90^o$ of ca 10.5 KJ/mol. According to published potential energy surfaces, the torsional angles observed for ortho-NO_2 groups in the solid state correspond to < 1 KJ/mol above the lowest energy conformation, and must be compensated by additional weak contacts within the lattice. Hence, any large changes upon compression must be compensated in energy by increase in other intermolecular contacts. The torsion angles calculated for the solid state structure at ambient pressure match well with the data obtained previously by both Vrcelj et al.[19] and Golovina et al.[20] Overall, it is found that τ3>τ1>τ2 is observed, with τ3(B)>τ3(A), τ2(B)>τ2(A) and τ1(B)<τ1(A), Figure 1. Hence, our solid-state DFT calculations support the previous experimental observations and confirm that the A and B conformations are slightly, albeit distinctly different. It can therefore be said that the PBE-D2 (and PBE-TS) calculations provide a good description of the molecular geometry. The torsion angles calculated at 5 GPa (see below) change only slightly as compared with the 0 GPa structure, Table 2. This is suggested to result from a lack in formation of strong intermolecular contacts upon compression in order to compensate for rotation of -NO_2 groups. It therefore follows that the Rietveld refinements for the elevated pressure diffraction data can be simplified by treating the TNT molecules (A and B) as rigid bodies

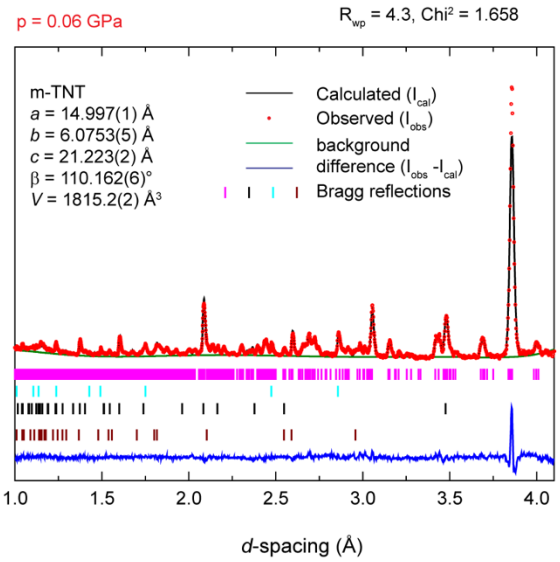

Figure 3 A representative Neutron diffraction pattern and Rietveld refinement fit of m-TNT at 0.06 GPa, experimental (obs) data are shown as red dots, the solid black and green line show the calculated profile from Rietveld refinement and background fit, respectively, and the bottom blue trace shows the residual intensity (I), I(obs)-I(calc). The simulated Bragg reflections for each phase are given as vertical lines; from top to bottom, m-TNT, Pb, Al_2O_3 and ZrO_2.

3.2 Hydrostatic Compression of monoclinic TNT

Neutron powder diffraction (NPD) patterns were collected for a sample of perdeuterated m-TNT across a pressure range 0.06(1) GPa → 5.25(2) GPa, ESI Figure S2.1. Rietveld refinement of the NPD pattern collected immediately after loading (at a load of 6 tonnes) confirmed that the sample did not react with moisture or air prior to loading, and also did not react with the pressure-transmitting medium, Figure 3. The additional reflections observed in the NPD patterns correspond to Pb (the pressure calibrant), Al_2O_3 (the gasket material), and ZrO_2 (the anvil material). Rietveld refinements were performed on diffraction patterns at each pressure point (ESI Figure S2.2). This allowed us to monitor the unit cell parameters and atomic positions with pressure, ESI Section S2 and S3.

Upon compression the unit-cell volume decreased significantly under low pressures, compressing by 7.7% at 1 GPa and by 12.1% at 2 GPa. This corresponds to over half of the total compression of the unit cell, which decreases in volume by 19.8% at 5.25 GPa. The compression is highly anisotropic, Figure 4a; the crystallographic *c*-axis is significantly more compressible than the a- and b axes (over the range 0 → 5.2 GPa, $V/V_0 = 0.802$, $a/a_0 = 0.948$, $b/b_0 = 0.937$, and $c/c_0 = 0.909$). This can be rationalized by noting that the c-axis lies perpendicular to the ABBA plane of molecules, and hence to the direction that contains the greatest void space. This anisotropic compressibility (Figure 4b) is consistent with previous reports from non-hydrostatic compression experiments.[13] In our current study, all three lattice parameters decrease continuously and show a smooth trend, Figure 4a. This indicates that no first order phase transitions take place between 0 and 5.25 GPa under hydrostatic conditions and differs from earlier reports of discontinuities in non-hydrostatic conditions, Figure 4(b). The compressibility of the corresponding principal axes (a unique set of orthogonal axes) with their direction of compression are shown in ESI Figure S5.

The compressibility of m-TNT was subsequently investigated by DFT methods and compared with NPD data, Figure 4c. Despite underestimating the ambient pressure structure by ca 3% (See Table 1), the compressibility of the unit cell obtained by PBE-D2 agrees well with experiment. The overall compressibility over the range 0 → 5 GPa shows $V/V_0 = 0.823$, with $a/a_0 = 0.951$, $b/b_0 = 0.935$ and $c/c_0 = 0.931$. The total compressibility differs from the experimental values by only 3%, which appears to be again mainly due to underestimating the crystallographic c-axis. Compressibility along the c-axis is slightly different between the PBE-D2 and NPD data, and this can be attributed to the fact that the directions of the principal axes compressions are not directly along the c-axis, and vary slightly between PBE-D2 and NPD (ESI, Figure S5). The pressure variation in the unit cell β-angle is well reproduced by the PBE-D2 method, albeit consistently overestimated by ca 1°. Nevertheless, differences in the experimentally determined angles are never more than ~1.5%.

While the PBE-TS method models the ambient pressure unit cell better than the PBE-D2 method (see Table 1), it performs only slightly better at predicting the compressibility of m-TNT. The overall PBE-TS compressibility from 0 → 5 GPa yields $V/V_0 = 0.818$, with $a/a_0 = 0.951$, $b/b_0 = 0.931$, and $c/c_0 = 0.927$, i.e. nearly identical compressibility as compared to the PBE-D2 data. The pressure variation in the unit-cell β-angle is also consistent with the values obtained from PBE-D2.

To determine which DFT dispersion correction scheme provides the best agreement of high pressure structures, we considered the DFT and experimental unit cells at the highest pressure points obtained. As pressure increased, the experimental and PBE-D2 unit cell parameters converged, (ESI Figure S4), with $V_{calc}/V_{exp} = 0.994$ at 5 GPa. The PBE-TS method consistently overestimates the unit cell at high pressure, with $V_{calc}/V_{exp} = 1.011$ at 5 GPa. This suggests that when temperature effects are negligible (e.g. at high pressure), the PBE-D2 method outperforms PBE-TS. The success of PBE-D2 has also been noted in RDX[47] and FOX-7.[10]

The unit cell undergoes ca 20% compression between 0-5 GPa. It is therefore of interest to consider the effect this change has on the intermolecular packing. Following on from the success of PBE-D2 at reproducing the high-pressure response of m-TNT, we.

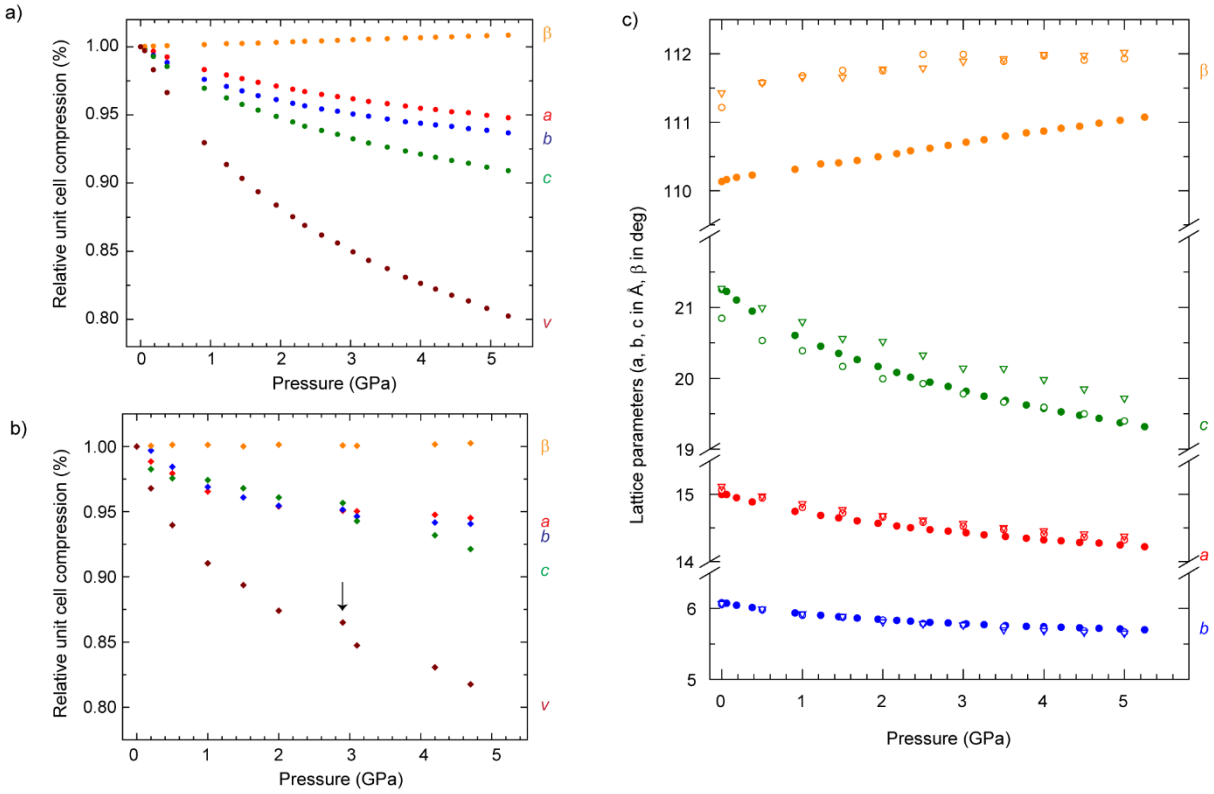

Figure 4 a) Relative unit cell compression (%) of m-TNT (perdeuterated) from current NPD study under hydrostatic condition, b) Relative unit cell compression (%) of m-TNT (hydrogenated) by Stevens et al.[Ref 22] , note the discontinuity at around 3 Gpa (marked by an arrow) is not observed at our current NPD data.; c) Lattice parameters of m-TNT as a function of hydrostatic pressure. Solid circles: NPD (current work), open circles: PBE-D2; open triangles: PBE-TS

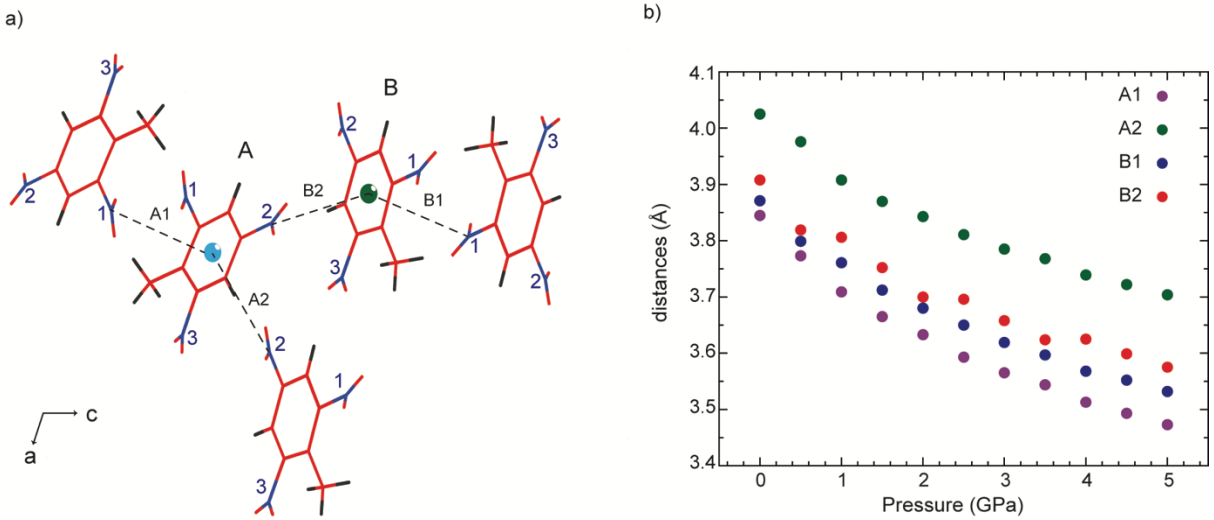

Figure 5 The effect of pressure on intermolecular contacts in m-TNT. a) Definition of selected intermolecular contacts between N…π-centroids.; b) Variation of intermolecular contacts as a function of pressure.

used this dataset to consider variations in the intermolecular distances upon compression, Figure 5. In both the A and B molecules, only two of the nitro groups participate in π···NO_2 interactions (N1 and N2 in Figures 1 and 5(a)). Interestingly, N3 (i.e that with the largest value of τ) does not participate in any of these interactions, leading to four unique π…NO_2 interactions within the unit cell, A1, A2, B1, and B2 as indicated in Figure 5(a). As the pressure increased, the values of all four distances decrease smoothly, and by approximately the same amount.

3.3 Hydrostatic Compression of orthorhombic TNT

This work presents the first experimental compression study of the metastable polymorph, o-TNT. The NPD patterns were collected from a sample of perdeuterated o-TNT from 0→5.1 GPa, with results of the unit cell parameters determined from Rietveld refinements

presented in Figure 6. The diffraction pattern obtained at each pressure point was refined using the same protocol as for m-TNT, as outlined in Section 2. All data sets were successfully refined as the o-TNT structure, ESI Figure S2.3. Upon compression, the experimental lattice parameters decreased smoothly, again suggesting that no first order phase transition occurs across this pressure range, Figure 6. The relative compressibility of the unit cell parameters are nearly identical to those found for m-TNT. The crystallographic *c*-axis is significantly more compressible than the a- and b-axes (over the range 0 → 5.1 GPa, $V/V_0 = 0.801$, $a/a_0 = 0.948$, $b/b_0 = 0.937$, and $c/c_0 = 0.903$). Direction of principal axes are along the crystallographic axes for o-TNT.

As with m-TNT, PBE-D2 underestimates the ambient pressure structure by ca. 4% (See Table 1). The compressibility of the unit cell axes from 0→5.0 GPa obtained by PBE-D2, however, agree well with experimental values: $V/V_0 = 0.825$, with $a/a_0 = 0.953$, $b/b_0 = 0.944$, and $c/c_0 = 0.917$. The crystallographic c-axis is again consistently underestimated at lower pressures, gradually converging to experimental values at higher pressures, Figure 6. At 5 GPa, the PBE-D2 volume is less than 0.6% lower than the experimental volume, and is therefore within experimental error. The PBE-TS method again performs better at ambient pressure as compared with PBE-D2. Despite this improvement at low pressure, the compressibility is again predicted to be nearly identical to that as obtained by PBE-D2: V/V0=0.817., with a\/a_0=0.953, b\/=0.930, and c\/c_o=0.921. Importantly, the unit cell volume obtained by PBE-TS at high pressure is in poorer agreement with experiment than the PBE-D2 method, with V_calc \/V_exp=0.995 for PBE-D2 and V_calc \/V_exp=1.012 for PBE-TS at 5 GPa. Thus again it is found that PBE-D2 offers an overall better description of the high pressure behavior of TNT.

As with m-TNT, the unit cell compressed by ca 20% between 0 and 5 GPa. Hence, marked changes can be expected in the intermolecular packing. With PBE-D2 again performing well against experimental lattice compression, we use these data to monitor changes in

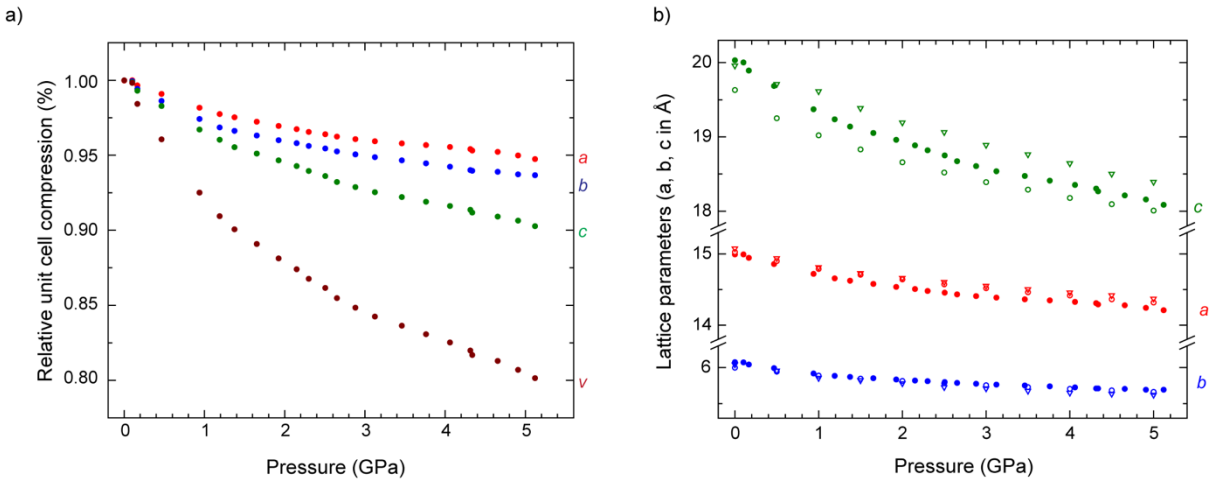

Figure 6 Relative unit cell compression (%) of o-TNT, b) Lattice parameters of o-TNT as a function of hydrostatic pressure. Solid circles: NPD (current work), open circles: PBE-D2; open triangles: PBE-TS..

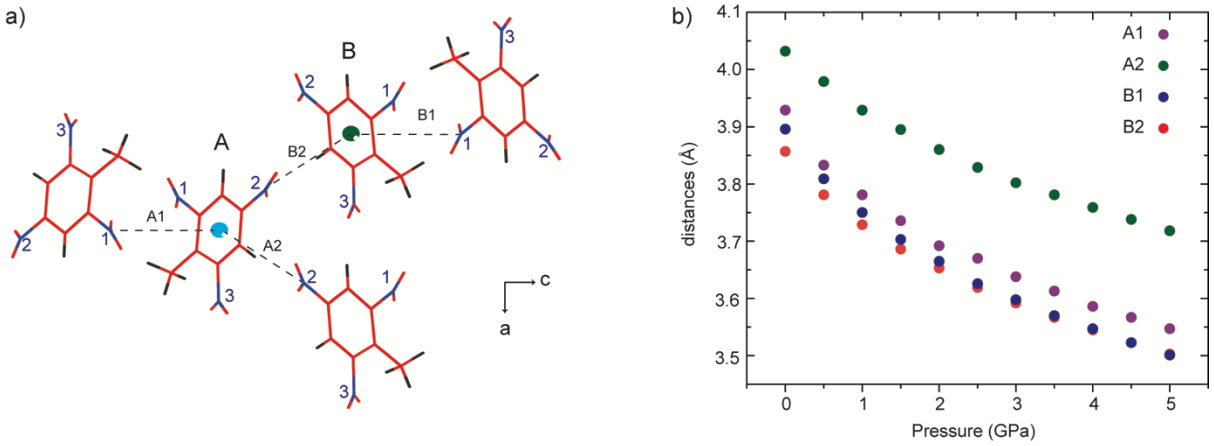

Figure 7 The effect of pressure on intermolecular contacts in o-TNT. a) Definition of selected intermolecular contacts between N…π-centroids.; b) Variation of intermolecular contacts as a function of pressure.

the intermolecular contacts of o-TNT with pressure, Figure 7. The same general trends are observed as for m-TNT; all of the intermolecular contacts shorten smoothly with pressure.

The high-pressure NPD study under hydrostatic conditions shows that both TNT polymorphs exhibit nearly identical compressibility. This can be rationalized by the similarity of the two structures, supporting the fact that the difference between these two forms is purely orientational in nature. For both forms, compression is dominated by a reduction in the interplanar spacing between layers of A and B molecules, corresponding to compression of the crystallographic c-axis.

3.4 The Equation of State for TNT Polymorphs

The equation of state (EoS) of EMs can be related to their detonation properties and have been suggested to offer insights into their response to impact.[48] Understanding the EoS is therefore an important factor for rationalizing their reactivity. Previous reports have suggested that computational approaches may be capable of providing accurate EoS,[47] and we explore this further here. The experimentally determined pressure-volume (P-V) curves for m-TNT and o-TNT are given in Figure 8. For each material, a smooth, monotonic decrease in volume is observed as a function of pressure, consistent with the trends observed in Figures 4 and 6. The variation in the experimental and calculated unit cell volumes as a function of pressure were fit to three semi-empirical EoS equations: third-order Birch–Murnaghan, fourth-order Birch-Murnaghan and the Vinet EOS. These equations relate the pressure, P, at a given volume, V, to the ambient pressure volume, V_o, the bulk modulus, B_0, and the derivative of the bulk modulus, B'. We note that the value of V_0 was not refined during EoS fitting, as this led to unreasonable results, particularly for o-TNT, ESI Table S6.

Visually, each of the three EoS forms appear to fit the P–V isotherms equally well; weighted chi^2 values can be found in ESI, Table S7. However, the three functions yield different bulk moduli (B_0) and its derivative (B'), Table 3. We noticed that using BM-4th order EOS on our data shows large uncertainties, and its use in the current study is not justified given the density of data points in the pressure range studied. Plot confidence ellipses indicate that the Vinet EoS provides B_0 and B' with the lowest uncertainties, and it is this EoS we show in Figure 8. The experimental B_0 values arising from the Vinet EOS fit, are respectively 8.93(7) and 7.91(21) for m- and o-TNT, with B' values of 9.24(10) and 10.29(31). Values of $B' > B_0$ indicates that the unit cell volumes decrease more rapidly at lower pressures and the material becomes stiffer with increasing pressure, as observed in Section 3.2. Experimental B_0 value for m-TNT is in excellent agreement with one of the previously reported studies (B_0 = 8.52 GPa, obtained by a Murnaghan fit to P-V/V_0 data under quasi-hydrostatic conditions up to 20 GPa.

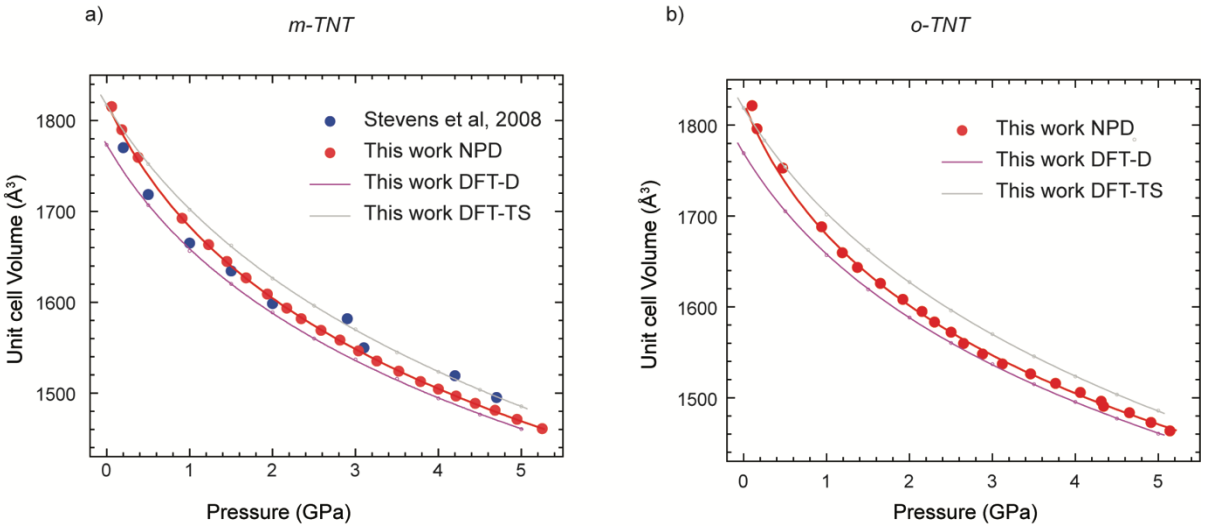

Figure 8 Unit cell volumes as a function of pressure for a) m-TNT and b) o-TNT; solid red circles: current NPD data, PBE-D2 and PBE-TS are shown with small open magenta circles and grey circles; both the NPD and DFT data are fitted with Vinet equation of state;; solid blue circles represent data from Stevens et al [ref 22]

Table 3: Comparison of bulk moduli (B_0) and its pressure-derivative (B′) determined from the EOS analyses of TNT. Approximate errors are shown for our work, and the experimental pressure and volume errors are also used to estimate the standard errors for calculated values. All values of B_o are given in GPa, and V_o are given in Å^3

m-TNT						
	Experiment (NPD)		Computation (PBE-D2)		Computation (PBE-TS)	
	V_0 = 1820.42 Å (not refined)		V_0 = 1773.31 Å (not refined)		V_0 = 1817.14 Å (not refined)	
	B_0 (GPa)	B′	B_0 (GPa)	B′	B_0 (GPa)	B′
Birch−Murnaghan 3rd order	8.53(12)	10.71(24)	10.87(11)	9.85(19)	12.1(3)	7.4(4)
Birch−Murnaghan 4th order	9.61(26)	7.1(7)	10.4(3)	11(1)	12.1(9)	7(2)
Vinet	8.93(7)	9.24(10)	11.18(11)	8.86(13)	12.1(3)	7.3(3)
o-TNT						
	Experiment (NPD)		Computation (PBE-D2)		Computation (PBE-TS)	
	V_0 = 1824.8 Å (not refined)		V_0 = 1769.18 Å (not refined)		V_0 = 1818.77 Å (not refined)	
	B_0 (GPa)	B′	B_0 (GPa)	B′	B_0 (GPa)	B′
Birch−Murnaghan 3rd order	7.3(3)	13.2(9)	11.4(3)	9.5(5)	12.0(3)	7.5(4)
Birch−Murnaghan 4th order	9(1)	7(3)	11(1)	11(3)	12.0(8)	7(2)
Vinet	7.91(21)	10.3(3)	11.7(3)	8.6(3)	12.1(3)	7.3(3)

with V_0 = 1828.8 Å^3).[12] In a more recent compression study using both hydrostatic and non-hydrostatic compression, a variety of B_0 values were reported, with values ranging from 7.3 to 12.8 GPa depending on the hydrostatic condition and the fitting form applied.[13]

The determined B_0 and B' obtained from fitting the unit cell volume obtained from the PBE-D2 and PBE-TS simulations are approximately similar to each other (Table 3). However, the determined values are higher than the experimentally derived values. The DFT calculations thus underestimate the compressibility of both TNT polymorphs. This is primarily a result of the initial underestimation of the unit-cell volume at ambient pressure in PBE-D, and the overestimation of the high-pressure volume in PBE-TS. The relative compressibility of the two polymorphs is also incorrectly predicted by DFT, with V_{mTNT}/V_{oTNT} of 1.13, 0.96 and 1.00 for NPD, DFT-D, and DFT-TS, respectively. We do however note that the discrepancy is small, and are negligible in terms of rationalizing the physical properties of the phases

It is undoubtedly important to conduct compression studies to the highest pressures practically attainable, since these compounds may experience very high pressures during detonation. However, our results confirm that, in order to obtain more precise determinations of the bulk modulus (B_0), it is also essential to obtain more high-quality diffraction data points at low pressures (< 1 GPa) under hydrostatic condition.

To summarize the discussion on TNT bulk moduli, o-TNT is found experimentally to be less compressible than m-TNT $(B_0(oTNT)/B_0(mTNT)$ =0.9. The standard deviations obtained from all the fitting EOSs are much lower than previous studies; the variation of bulk moduli are also within 1 GPa between the three fitting EOSs used. Unfortunately, despite DFT

methods proving capable of accurate prediction of the bulk moduli of other nitro-based EMs,[10] the DFT-D derived values of B_o and B′ were overestimated for TNT. We suggest this to be primarily due to the large thermal expansion of TNT, as compared to other materials, such as the hydrogen-bonded material FOX-7, for which bulk moduli was more closely reproduced (i.e. within 1 GPa; ca 5%) by DFT-D.[10]

CONCLUSIONS

This work reports the effects of hydrostatic compression on the crystal structure of two known polymorphs of TNT, from neutron powder diffraction data, and represents the first example of a high pressure study for o-TNT. The compression trend observed was in excellent agreement with the hydrostatic compression trend predicted by the PBE-D2 method. The pressure−volume curve can be fitted to a Birch−Murnaghan equation of state (both 3rd order and 4th order) and also a Vinet equation of state, with the latter providing the lowest standard deviations. The bulk moduli obtained are 8.93(7) and 7.91(21) GPa for monoclinic and orthorhombic forms of TNT, respectively. PBE-D2 overestimates the bulk modulus of both the forms due to underestimating the volume at ambient pressure at 0 K. The neutron powder diffraction study failed to find any evidence for a phase transition at ∼2-4 GPa previously suspected from angle dispersive X-ray diffraction[22] and vibrational spectroscopy measurements.[23] Although we cannot discount the potential effects of sample deuteration, we believe that the discrepancy arises due to the non-hydrostatic compression conditions applied in the previous studies. The structural data presented herein are illustrative of a significant advance in the structural characterization of this molecular materials under extreme conditions. The level of complexity of the TNT molecule extends the limits to which high-pressure techniques may be applied, and these results will be of importance not only to the energetics community but also to solid-state chemists and physicists wishing to model the behavior of this important class of nitro-aromatic energetic material.

ASSOCIATED CONTENT

Figure S1 displays ^{1}H-NMR spectrum of deuterated TNT; Figure S2.1 displays Sequence of NPD patterns obtained for both perdeuterated m-TNT and o-TNT upon increasing pressure; Figure S2.2 & Figure S2.3 display Rietveld refinements of the NPD patterns obtained at elevated pressures for m-TNT and o-TNT, respectively; Table S3.1 – S3.4 show variation of unit cell parameters of both m-TNT and o_TNT with pressure,. Figure S4 shows comparison of unit cell volumes as obtained from experiment and calculations at 5 GPa; Figure S5 displays comparison of compression of principle axes of m-TNT; Table S6 provides experimental bulk modulus when V_0 refined Table S7 provides Weighted chi2 values of the EoS fits of NPD data. This material is available free of charge via the Internet at http://pubs.acs.org.

AUTHOR INFORMATION

Corresponding Author

***E-mail: sumit.konar@ed.ac.uk**

ORCID

Sumit Konar: 0000-0003-3156-6536
Adam A. L. Michalchuk: 0000-0001-7405-3269
Nilgun Sen: 0000-0002-1997-1312
Craig L. Bull: 0000-0002-5170-6674
Carole A. Morrison: 0000-0002-5489-7111
Colin Pulham: 0000-0002-3689-9594

Author Contributions

The manuscript was written through contributions of all authors. All authors have given approval to the final version of the manuscript.

Notes

The authors declare no competing financial interest.

ACKNOWLEDGMENT

All neutron powder diffraction data were collected on the PEARL beamline at ISIS Neutron and Muon Source (RB 1720337). We thank Nicholas Funnell and Christopher Ridley (ISIS, STFC) for their help in performing the high pressure neutron experiments on PEARL. We are grateful to the UK Materials and Molecular Modelling Hub for computational resources, which is partially funded by EPSRC (EP/P020194/1). The authors thank EPSRC CMAC EP/I033459/1 (AM) and the TUBITAK-BIDEB 2219-International Postdoctoral Research Fellowship Program (NS) for financial support. Further thanks are given to the Edinburgh Compute and Data Facilities (ECDF) for additional computational resources.

References

(1) Akhavan, J. *The Chemistry of Explosives*; 2011.

(2) Tsyshevsky, R.; Sharia, O.; Kuklja, M.; Tsyshevsky, R. V.; Sharia, O.; Kuklja, M. M. Molecular Theory of Detonation Initiation: Insight from First Principles Modeling of the Decomposition Mechanisms of Organic Nitro Energetic Materials. *Molecules* **2016**, *21* (2), 236. https://doi.org/10.3390/molecules21020236.

(3) Bernstein, J. Ab Initio Study of Energy Transfer Rates and Impact Sensitivities of Crystalline Explosives. *J. Chem. Phys.* **2018**, *148* (8), 084502. https://doi.org/10.1063/1.5012989.

(4) Michalchuk, A. A. L.; Fincham, P. T.; Portius, P.; Pulham, C. R.; Morrison, C. A. A Pathway to the Athermal Impact Initiation of Energetic Azides. *J. Phys. Chem. C* **2018**, *122* (34), 19395–19408. https://doi.org/10.1021/acs.jpcc.8b05285.

(5) Kuklja, M. M.; Rashkeev, S. N. Shear-Strain-Induced Chemical Reactivity of Layered

Molecular Crystals. *Appl. Phys. Lett.* **2007**, *90* (15), 151913. https://doi.org/10.1063/1.2719031.
(6) Zhang, J.; Mitchell, L. A.; Parrish, D. A.; Shreeve, J. M. Enforced Layer-by-Layer Stacking of Energetic Salts towards High-Performance Insensitive Energetic Materials. *J. Am. Chem. Soc.* **2015**, *137* (33), 10532–10535. https://doi.org/10.1021/jacs.5b07852.
(7) Yuan, B.; Yu, Z.; Bernstein, E. R. Initial Decomposition Mechanism for the Energy Release from Electronically Excited Energetic Materials: FOX-7 (1,1-Diamino-2,2-Dinitroethene, C2H4N4O4). *J. Chem. Phys.* **2014**, *140* (7), 074708. https://doi.org/10.1063/1.4865266.
(8) Chakraborty, D.; Muller, R. P.; Dasgupta, S.; Goddard, W. A. Mechanism for Unimolecular Decomposition of HMX (1,3,5,7-Tetranitro-1,3,5,7-Tetrazocine), an Ab Initio Study. *J. Phys. Chem. A* **2001**, *105* (8), 1302–1314. https://doi.org/10.1021/jp0026181.
(9) Mathieu, D.; Alaime, T. Predicting Impact Sensitivities of Nitro Compounds on the Basis of a Semi-Empirical Rate Constant. *J. Phys. Chem. A* **2014**, *118* (41), 9720–9726. https://doi.org/10.1021/jp507057r.
(10) Hunter, S.; Coster, P. L.; Davidson, A. J.; Millar, D. I. A.; Parker, S. F.; Marshall, W. G.; Smith, R. I.; Morrison, C. A.; Pulham, C. R. High-Pressure Experimental and DFT-D Structural Studies of the Energetic Material FOX-7. *J. Phys. Chem. C* **2015**, *119* (5), 2322–2334. https://doi.org/10.1021/jp5110888.
(11) Millar, D. I. A.; Maynard-Casely, H. E.; Kleppe, A. K.; Marshall, W. G.; Pulham, C. R.; Cumming, A. S. Putting the Squeeze on Energetic Materials-Structural Characterisation of a High-Pressure Phase of CL-20. *Crystengcomm* **2010**, *12* (9), 2524–2527. https://doi.org/10.1039/c002701d.
(12) ASAY, B. W.; HENSON, B. F.; SMILOWITZ, L. B.; DICKSON, P. M. On the Difference in Impact Sensitivity of Beta and Delta HMX. *J. Energ. Mater.* **2003**, *21* (4), 223–235. https://doi.org/10.1080/713770434.
(13) Yoo, C.-S.; Cynn, H. Equation of State, Phase Transition, Decomposition of β-HMX (Octahydro-1,3,5,7-Tetranitro-1,3,5,7-Tetrazocine) at High Pressures. *J. Chem. Phys.* **1999**, *111* (22), 10229–10235. https://doi.org/10.1063/1.480341.
(14) Goetz, F.; Brill, T. B.; Ferraro, J. R. Pressure Dependence of the Raman and Infrared Spectra of .Alpha.-, .Beta.-, .Gamma.-, and .Delta.-Octahydro-1,3,5,7-Tetranitro-1,3,5,7-Tetrazocine. *J. Phys. Chem.* **1978**, *82* (17), 1912–1917. https://doi.org/10.1021/j100506a011.
(15) Oswald, I. D. H.; Millar, D. I. A.; Davidson, A. J.; Francis, D. J.; Marshall, W. G.; Pulham, C. R.; Cumming, A.; Lennie, A. R.; Warren, J. E. High-Pressure Structural Studies of Energetic Compounds. *High Press. Res.* **2010**, *30* (2), 280–291. https://doi.org/10.1080/08957951003757903.
(16) Dreger, Z. A.; Gupta, Y. M. High Pressure Raman Spectroscopy of Single Crystals of Hexahydro-1,3,5-Trinitro-1,3,5-Triazine (RDX). *J. Phys. Chem. B* **2007**, *111* (15), 3893–3903. https://doi.org/10.1021/jp0681092.
(17) Millar, D. I. A.; Oswald, I. D. H.; Barry, C.; Francis, D. J.; Marshall, W. G.; Pulham, C. R.; Cumming, A. S. Pressure-Cooking of Explosives—the Crystal Structure of ε-RDX as Determined by X-Ray and Neutron Diffraction. *Chem. Commun.* **2010**, *46* (31), 5662–5664. https://doi.org/10.1039/C0CC00368A.
(18) Stevens, L. L.; Velisavljevic, N.; Hooks, D. E.; Dattelbaum, D. M. Hydrostatic Compression Curve for Triamino-Trinitrobenzene Determined to 13.0 GPa with Powder X-Ray Diffraction. *Propellants Explos. Pyrotech.* **2008**, *33* (4), 286–295. https://doi.org/10.1002/prep.200700270.
(19) Vrcelj, R. M.; Sherwood, J. N.; Kennedy, A. R.; Gallagher, H. G.; Gelbrich, T. Polymorphism in 2-4-6 Trinitrotoluene. *Cryst. Growth Des.* **2003**, *3* (6), 1027–1032. https://doi.org/10.1021/cg0340704.
(20) Golovina, N. I.; Titkov, A. N.; Raevskii, A. V.; Atovmyan, L. O. Kinetics and Mechanism of Phase Transitions in the Crystals of 2,4,6-Trinitrotoluene and Benzotrifuroxane. *J. Solid State Chem.* **1994**, *113* (2), 229–238. https://doi.org/10.1006/jssc.1994.1365.
(21) Ravi, P.; Badgujar, D. M.; Gore, G. M.; Tewari, S. P.; Sikder, A. K. Review on Melt Cast Explosives. *Propellants Explos. Pyrotech.* **2011**, *36* (5), 393–403. https://doi.org/10.1002/prep.201100047.
(22) Stevens, L. L.; Velisavljevic, N.; Hooks, D. E.; Dattelbaum, D. M. The High-Pressure Phase Behavior and Compressibility of 2,4,6-Trinitrotoluene. *Appl. Phys. Lett.* **2008**, *93* (8), 081912. https://doi.org/10.1063/1.2973162.
(23) Bowden, P. R.; Chellappa, R. S.; Dattelbaum, D. M.; Manner, V. W.; Mack, N. H.; Liu, Z. The High-Pressure Phase Stability of 2,4,6-Trinitrotoluene (TNT). *J. Phys. Conf. Ser.* **2014**, *500* (5), 052006. https://doi.org/10.1088/1742-6596/500/5/052006.
(24) Tokmakoff, A.; Fayer, M. D.; Dlott, D. D. Chemical Reaction Initiation and Hot-Spot Formation in Shocked Energetic Molecular Materials. *J. Phys. Chem.* **1993**, *97* (9), 1901–1913. https://doi.org/10.1021/j100111a031.
(25) Henderson, C.; Coster, P.; Marshall, W.; Maynard-Casley, H.; Pulham, C. High-Pressure Neutron Diffraction: A Gentler Way to Study Explosives. *Acta Crystallogr. A* **2013**, *69* (a1), 612–612. https://doi.org/10.1107/S0108767313094671.
(26) Byrd, E. F. C.; Rice, B. M. Ab Initio Study of Compressed 1,3,5,7-Tetranitro-1,3,5,7-Tetraazacyclooctane (HMX), Cyclotrimethylenetrinitramine (RDX), 2,4,6,8,10,12-Hexanitrohexaazaisowurzitane (CL-20), 2,4,6-Trinitro-1,3,5-Benzenetriamine (TATB), and Pentaerythritol Tetranitrate (PETN). *J. Phys. Chem. C* **2007**, *111* (6), 2787–2796. https://doi.org/10.1021/jp0617930.
(27) Sorescu, D. C.; Rice, B. M. Theoretical Predictions of Energetic Molecular Crystals at Ambient and Hydrostatic Compression

Conditions Using Dispersion Corrections to Conventional Density Functionals (DFT-D). *J. Phys. Chem. C* **2010**, *114* (14), 6734–6748. https://doi.org/10.1021/jp100379a.

(28) Bull, C. L.; Funnell, N. P.; Tucker, M. G.; Hull, S.; Francis, D. J.; Marshall, W. G. PEARL: The High Pressure Neutron Powder Diffractometer at ISIS. *High Press. Res.* **2016**, 1–19. https://doi.org/10.1080/08957959.2016.1214730.

(29) Besson, J. M.; Nelmes, R. J.; Hamel, G.; Loveday, J. S.; Weill, G.; Hull, S. Neutron Powder Diffraction above 10 GPa. *Phys. B Condens. Matter* **1992**, *180–181*, 907–910. https://doi.org/10.1016/0921-4526(92)90505-M.

(30) Marshall, W. G.; Francis, D. J. Attainment of Near-Hydrostatic Compression Conditions Using the Paris–Edinburgh Cell. *J. Appl. Crystallogr.* **2002**, *35* (1), 122–125.

(31) Klotz, S.; Philippe, J.; Cochard, E. Solidification and Viscosity of Iso-Pentane/n-Pentane Mixtures at Low Temperatures and High Pressure. *J. Phys. Appl. Phys.* **2006**, *39* (8), 1674–1677. https://doi.org/10.1088/0022-3727/39/8/029.

(32) Strässle, Th.; Klotz, S.; Kunc, K.; Pomjakushin, V.; White, J. S. Equation of State of Lead from High-Pressure Neutron Diffraction up to 8.9 GPa and Its Implication for the NaCl Pressure Scale. *Phys. Rev. B* **2014**, *90* (1), 014101. https://doi.org/10.1103/PhysRevB.90.014101.

(33) Arnold, O.; Bilheux, J. C.; Borreguero, J. M.; Buts, A.; Campbell, S. I.; Chapon, L.; Doucet, M.; Draper, N.; Ferraz Leal, R.; Gigg, M. A.; et al. Mantid—Data Analysis and Visualization Package for Neutron Scattering and μ SR Experiments. *Nucl. Instrum. Methods Phys. Res. Sect. Accel. Spectrometers Detect. Assoc. Equip.* **2014**, *764*, 156–166. https://doi.org/10.1016/j.nima.2014.07.029.

(34) Larson, A. C.; Von Dreele, R. B. *General Structure Analysis System (GSAS)*; Los Alamos National Laboratory Report LAUR 86-748, 2004.

(35) Cliffe, M. J.; Goodwin, A. L. PASCal: A Principal Axis Strain Calculator for Thermal Expansion and Compressibility Determination. *J. Appl. Crystallogr.* **2012**, *45* (6), 1321–1329. https://doi.org/10.1107/S0021889812043026.

(36) Clark, S. J.; Segall, M. D.; Pickard, C. J.; Hasnip, P. J.; Probert, M. I. J.; Refson, K.; Payne, M. C. First Principles Methods Using CASTEP. *Z. Für Krist. - Cryst. Mater.* **2009**, *220* (5/6), 567–570. https://doi.org/10.1524/zkri.220.5.567.65075.

(37) Perdew, J. P.; Burke, K.; Ernzerhof, M. Generalized Gradient Approximation Made Simple. *Phys. Rev. Lett.* **1996**, *77* (18), 3865–3868. https://doi.org/10.1103/PhysRevLett.77.3865.

(38) Grimme, S. Semiempirical GGA-Type Density Functional Constructed with a Long-Range Dispersion Correction. *J. Comput. Chem.* **2006**, *27* (15), 1787–1799. https://doi.org/10.1002/jcc.20495.

(39) Tkatchenko, A.; Scheffler, M. Accurate Molecular Van Der Waals Interactions from Ground-State Electron Density and Free-Atom Reference Data. *Phys. Rev. Lett.* **2009**, *102* (7), 073005. https://doi.org/10.1103/PhysRevLett.102.073005.

(40) Monkhorst, H. J.; Pack, J. D. Special Points for Brillouin-Zone Integrations. *Phys. Rev. B Solid State* **1976**, *13* (12), 5188–5192. https://doi.org/10.1103/PhysRevB.13.5188.

(41) Grimme, S.; Antony, J.; Ehrlich, S.; Krieg, H. A Consistent and Accurate Ab Initio Parametrization of Density Functional Dispersion Correction (DFT-D) for the 94 Elements H-Pu. *J. Chem. Phys.* **2010**, *132* (15), 154104. https://doi.org/10.1063/1.3382344.

(42) Caldeweyher, E.; Ehlert, S.; Hansen, A.; Neugebauer, H.; Spicher, S.; Bannwarth, C.; Grimme, S. A Generally Applicable Atomic-Charge Dependent London Dispersion Correction. *J. Chem. Phys.* **2019**, *150* (15), 154122. https://doi.org/10.1063/1.5090222.

(43) Gallagher, H. G.; Sherwood, J. N. Polymorphism, Twinning and Morphology of Crystals of 2,4,6-Trinitrotoluene Grown from Solution. *J. Chem. Soc. Faraday Trans.* **1996**, *92* (12), 2107–2116. https://doi.org/10.1039/FT9969202107.

(44) Clarkson, J.; Smith, W. E.; Batchelder, D. N.; Smith, D. A.; Coats, A. M. A Theoretical Study of the Structure and Vibrations of 2,4,6-Trinitrotolune. *J. Mol. Struct.* **2003**, *648* (3), 203–214. https://doi.org/10.1016/S0022-2860(03)00024-3.

(45) Azuri, I.; Hirsch, A.; Reilly, A. M.; Tkatchenko, A.; Kendler, S.; Hod, O.; Kronik, L. Terahertz Spectroscopy of 2,4,6-Trinitrotoluene Molecular Solids from First Principles. *Beilstein J. Org. Chem.* **2018**, *14* (1), 381–388. https://doi.org/10.3762/bjoc.14.26.

(46) Erba, A.; Maul, J.; Civalleri, B. Thermal Properties of Molecular Crystals through Dispersion-Corrected Quasi-Harmonic Ab Initio Calculations: The Case of Urea. *Chem. Commun.* **2016**, *52* (9), 1820–1823. https://doi.org/10.1039/C5CC08982D.

(47) Hunter, S.; Sutinen, T.; Parker, S. F.; Morrison, C. A.; Williamson, D. M.; Thompson, S.; Gould, P. J.; Pulham, C. R. Experimental and DFT-D Studies of the Molecular Organic Energetic Material RDX. *J. Phys. Chem. C* **2013**, *117* (16), 8062–8071. https://doi.org/10.1021/jp4004664.

(48) Bondarchuk, S. V. Quantification of Impact Sensitivity Based on Solid-State Derived Criteria. *J. Phys. Chem. A* **2018**, *122* (24), 5455–5463. https://doi.org/10.1021/acs.jpca.8b01743.